Available online at www.sciencedirect.com
ScienceDirect
C. R. Chimie 11 (2008) 875–889
COMPTES RENDUS CHIMIE
http://france.elsevier.com/direct/CRAS2C/

Full paper / Mémoire

Tuning the electronic properties of Fe_2(μ-arenedithiolate)$(CO)_{6-n}(PMe_3)_n$ ($n = 0, 2$) complexes related to the [Fe–Fe]-hydrogenase active site

Lennart Schwartz [a], Pradyumna S. Singh [a], Lars Eriksson [b], Reiner Lomoth [a], Sascha Ott [a,*]

[a] *Department of Photochemistry and Molecular Science, Uppsala University, Box 523, 751 20 Uppsala, Sweden*
[b] *Division of Structural Chemistry, Arrhenius Laboratory, Stockholm University, 106 91 Stockholm, Sweden*

Received 11 February 2008; accepted after revision 7 April 2008
Available online 2 June 2008

Abstract

Complexes $[Fe_2(\mu\text{-}S_2Ar)(CO)_6]$ (S_2Ar) = benzene-1,2-dithiolate (**1a**) toluene-3,4-dithiolate (**2a**), 3,6-dichloro-1,2-benzenedithiolate (**3a**), quinoxaline-2,3-dithiolate (**7a**) have been prepared to investigate the electronic effect that different bridging arenedithiolate ligands have on the appended $Fe_2(CO)_6$ sites. Dinuclear complexes $[Fe_2(\mu\text{-}S_2Ar)(CO)_4(PMe_3)_2]$ (**1–3,7)b** and mononuclear complexes $[Fe(S_2Ar)(CO)_2(PMe_3)_2]$ (**1–3,7)c** were synthesized from their parent hexacarbonyl complexes (**1–3,7)a**. IR spectroscopic, crystallographic and electrochemical analyses show that an increase of the electron-withdrawing character (where quinoxaline-2,3-dithiolate > 3,6-dichloro-1,2-benzenedithiolate > 1,2-benzenedithiolate ≥ toluene-3,4-dithiolate) of the bridging ligand leads to a decreased electron density at the iron centers, which yield a milder reduction potential and higher eCO stretching frequencies. This effect is coherent for all of the investigated complexes. Electrocatalytic proton reduction by complex **3a** (with trifluoromethanesulfonic acid) was evidenced by cyclic voltammetry. As a result of the milder reduction potential of **3a** itself, proton reduction that is promoted by **3a** proceeds at a potential that is milder than that for the **1a**-catalyzed process. ***To cite this article: L. Schwartz et al., C. R. Chimie 11 (2008).***

Keywords: Bioinorganic chemistry; Electrochemistry; IR spectroscopy; Hydrogen production

1. Introduction

[Fe–Fe]-hydrogenases are enzymes which can catalyze the reversible reduction of protons to molecular hydrogen [1]. Having been selected by nature over millions of years of evolution, hydrogenases provide inspiration and knowledge on how an efficient proton reduction catalyst should be designed. After structure elucidation of two [Fe–Fe]-hydrogenases by X-ray crystallography [2,3] (Fig. 1), a variety of close mimics of their active sites have been synthesized [4–11]. In this context, $[Fe_2(\mu\text{-bdt})(CO)_6]$ (bdt = 1,2-benzenedithiolate) (**1a**) has recently been shown to catalyze the reduction of *p*-toluenesulfonic acid (pK_a ~8.7 in CH_3CN [12]) [13] at relatively mild potential and the reduction of weaker acids (AcOH, pK_a ~22.3 in CH_3CN [12]) at mild overpotential [14]. Furthermore, complex **1a** has proven

* Corresponding author.
E-mail address: sascha.ott@fotomol.uu.se (S. Ott).

1631-0748/$ - see front matter © 2008 Académie des sciences. Published by Elsevier Masson SAS. All rights reserved.
doi:10.1016/j.crci.2008.04.001

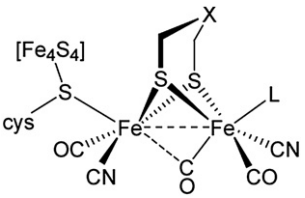

Fig. 1. Schematic view of the [Fe–Fe]-hydrogenase active site (the H-cluster). X = NH or O or CH_2, L = H_2O, CO, H or vacant site.

to be a good candidate for mechanistic investigations of the catalytic cycle as its electrochemistry is generally well behaved with reversible waves in the cyclic voltammograms in the absence of acids. All of these features can be explained by an interaction between the sulfur p_π orbitals and the benzene p_π orbitals which buffers the electron content at the diiron centre and minimizes the energy changes upon reduction [15–17].

Being inspired by the favorable properties that have been reported for complex **1a**, we were intrigued by the possibility to modulate the electronic content of the arenedithiolate ligand and to investigate the effect on the appended diiron site by spectroscopic, crystallographic and electrochemical techniques. Furthermore, we synthesized $[Fe_2(\mu\text{-}S_2Ar)(CO)_4(PMe_3)_2]$ analogues from the parent hexacarbonyl complexes to study the interplay between electron-donating phosphine ligands and electron-withdrawing arenedithiolates.

2. Results and discussion

2.1. Preparation and spectroscopic characterization

Complexes $[Fe_2(\mu\text{-}S_2R)(CO)_6]$ S_2R = benzene-1,2-dithiolate (**1a**) [18,19], toluene-3,4-dithiolate (**2a**) [20,21] and 3,6-dichloro-1,2-benzenedithiolate (**3a**) were prepared from $Fe_3(CO)_{12}$ and the respective dithiol in toluene at reflux (Scheme 1). The reactions were followed by TLC analysis and terminated when all $Fe_3(CO)_{12}$ was consumed. While complexes **1a** and **2a** were obtained in acceptable yields (57 and 51% respectively), complex **3a** could only be prepared in 25% yield. Since a sizeable amount of decomposed material is observed during the course of this reaction, it seems that complex **3a** is less stable than **1a** and **2a** under the reaction conditions. The observed lower stability of complex **3a** can be rationalized by the presence of weaker Fe–S bonds that are caused by the decreased electron content of the bridging 3,6-dichloro-1,2-benzenedithiolate ligand. While the reactions of complexes **1a** and **2a** were completed after 75–90 min, the synthesis of **3a** required only 45 min. The ^1H NMR and ^{13}C NMR spectral data of **1a** and **2a** are in agreement with the literature data. The ^1H NMR spectrum of **3a** exhibits one singlet for the two aromatic protons at 6.63 ppm. The $^{13}C\{^1H\}$ NMR spectrum features the three aromatic carbon signals and one signal for the carbonyl ligands at 206.9 ppm.

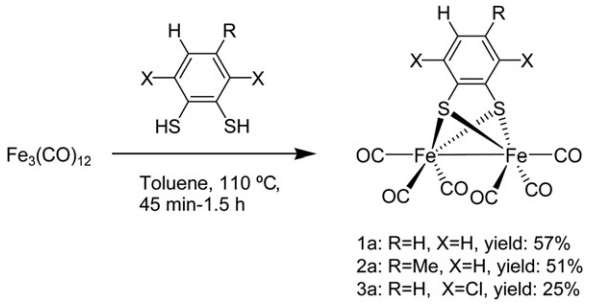

Scheme 1.

Complexes (**1–3**)**a** were separately treated with 10 equiv. of trimethylphosphine in argon-degassed hexane to obtain complexes (**1–3**)**b** in acceptable yields (Scheme 2) [22]. Interestingly, mononuclear byproducts **1c** [23,24], **2c** and **3c** were also formed in moderate yields. Rauchfuss and co-workers have presented a cyanide derivate of **1c**, namely $[Fe(bdt)(CN)_2(CO)_2]^{2-}$ [25]. The dinuclear complexes could successfully be separated from the mononuclear compounds by flash column chromatography. During the purification procedures, a third product could be isolated that was identical independent from which of the three reactions it had been obtained from. This white solid was identified as $[Fe(CO)_3(PMe_3)_2]$ by X-ray diffraction analysis.

Dinuclear (**1–3**)**b** and mononuclear (**1–3**)**c** complexes were characterized by ^1H, ^{13}C and ^{31}P NMR spectroscopies. The ^1H NMR spectra of **1b**, **2b** and **3b** exhibit doublets ($^2J_{H-P}$ = 8.8, 9.2, 9.2 Hz, respectively) for the methyl protons of the PMe_3 ligands. The $^{31}P\{^1H\}$ NMR spectra show only one resonance signal (δ = 20.9, 21.1, 21.2 ppm, respectively) for each compound and thus reveal that the PMe_3 ligands are equivalent in all dinuclear complexes. The $^{13}C\{^1H\}$ NMR spectra for complexes **1b**, **2b** and **3b** reveal doublets for the methyl carbons at δ = 20.8, 20.8, 21.0 ppm, respectively (J_{C-P} = 26.1, 26.9, 26.9 Hz, respectively). Furthermore, the carbonyl carbons feature as doublets at δ = 216.4, 216.5 and 215.8 ppm ($^2J_{C-P}$ = 10.8, 10.8, 10.8 Hz, respectively) for complexes **1b**, **2b** and **3b**, indicating that the carbonyl carbons only couple to the phosphorus of the same $Fe(CO)_2(PMe_3)$ subunit.

The $^{31}P\{^1H\}$ NMR spectra of mononuclear complexes **1c**, **2c** and **3c** feature singlet resonances at

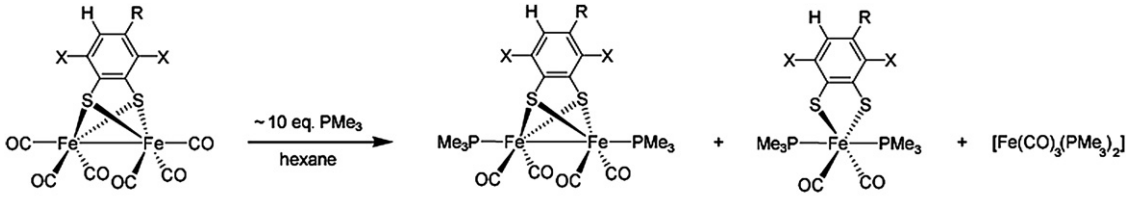

Scheme 2.

$\delta = 11.3$, 11.2 and 11.9 ppm, respectively, indicating that the PMe_3 ligands are equivalent. The ^1H NMR spectra of **1c**, **2c** and **3c** show virtual triplets [26–28] for the methyl protons at $\delta = 1.45$, 1.45 and 1.47 ppm, respectively. The $^{13}C\{^1H\}$ NMR spectra show similar virtual triplet patterns for the PMe_3 methyl carbons in complexes **1c**, **2c** and **3c** at $\delta = 14.4$, 14.5 and 14.4 ppm, respectively. Moreover, the carbonyl carbons give rise to triplets resonances in complexes **1c** and **3c** at $\delta = 211.3$ and 210.7 ppm ($^2J_{C-P} = 21.5$ Hz and $^2J_{C-P} = 22.3$ Hz), respectively. The NMR spectra thus indicate that the two PMe_3 ligands are in a *trans* position and that the phosphorus atoms are equivalent. The carbonyl ligands in complex **2c** are not chemically equivalent as the methyl substituent on the benzenedithiolate ligand breaks the C_{2V} symmetry that is found in **1c** and **3c**. Therefore, the $^{13}C\{^1H\}$ NMR spectrum of **2c** features two triplets with similar coupling constants ($^2J_{C-P} = 21.1$ Hz) very close to each other at $\delta = 211.3$. The triplet patterns of the two signals indicate the same coordination geometry of the PMe_3 and CO ligands as in **1c** and **3c**.

The carbonyl region of the IR spectra for complexes (**1–3**)**a**, (**1–3**)**b** and (**1–3**)**c** is presented in Fig. 2a–c. The IR spectra of the hexacarbonyl complexes **1a** and **2a** (Fig. 2a) show that the methyl group in the toluene-3,4-dithiolate ligand does not affect the electronic properties of the latter complex. However, the electronic effect of the electron-withdrawing chloride substituents of the 3,6-dichloro-1,2-benzenedithiolate ligand in **3a** is communicated through the entire complex. The lower electron density at the iron centers results in less backbonding into the π^*-orbital of the CO ligands which leads to a shift of the CO stretching frequencies by $\Delta\upsilon_{CO} = \sim 6\ cm^{-1}$ towards higher energy. As a result of the electron-donating phosphine ligands, the IR spectra of (**1–3**)**b** (Fig. 2b) are shifted by $\upsilon_{CO} = 55\ cm^{-1}$ towards lower energy compared to their hexacarbonyl analogues. This shift is somewhat less than expected as the carbonyl bands of $Fe_2(\mu\text{-pdt})(CO)_4(PMe_3)_2$ are shifted by almost $100\ cm^{-1}$ compared to the parent hexacarbonyl complexes [29]. The IR spectra of complexes (**1–3**)**b** follow the same trend as the hexacarbonyl complexes (**1–3**)**a** with the bands for complex **3b** being shifted by $\Delta\upsilon_{CO} = \sim 6\ cm^{-1}$ compared to those of **1b** and **2b**. The carbonyl stretching frequencies in the IR spectra of complexes (**1–3**)**c** (Fig. 2c) are located between those of complexes (**1–3**)**a** and (**1–3**)**b**. As the number of CO ligands is less in complexes (**1–3**)**c**, the number of stretching modes is decreased and a simpler IR spectrum is obtained. Again, the electron-withdrawing character of the 3,6-dichloro-1,2-benzenedithiolate ligand gives rise to higher energy CO stretch frequencies.

Having established that substitutions on the arene moiety in (**1–3**)**a**, (**1–3**)**b** and (**1–3**)**c** can affect the electron density at the diiron core, we were interested to explore other complexes with aromatic bridging ligands. This prompted us to study iron complexes with larger aromatic dithiolate units; *i.e.* quinoxalines. The *N*-heteroatoms in quinoxalines offer basic sites that can potentially be protonated which would further reduce the electron-donating capacity of the ligand. Therefore, we set out to synthesize compound **7a** (Scheme 3). Quinoxaline-2,3-dione **4** can easily be prepared in large quantities [30]. Quinoxaline-2,3-dithiol (**6**) was prepared from 2,3-dichloroquinoxaline [31] (**5**) as described previously [32]. Compound **6** was reacted with $Fe_3(CO)_{12}$ in THF at reflux to obtain **7a** in low yield (15%). Again, the low yield may be rationalized by the strong electron-withdrawing character of the 2,3-dithiolatoquinoxaline ligand, and the associated decreased Fe–S bond strength in complex **7a**. In the synthesis of **7a**, the reaction time is shorter compared to those required for the synthesis of (**1–3**)**a**. It seems that more electron-withdrawing arenedithiolate ligands result in faster reaction rates for the complexation

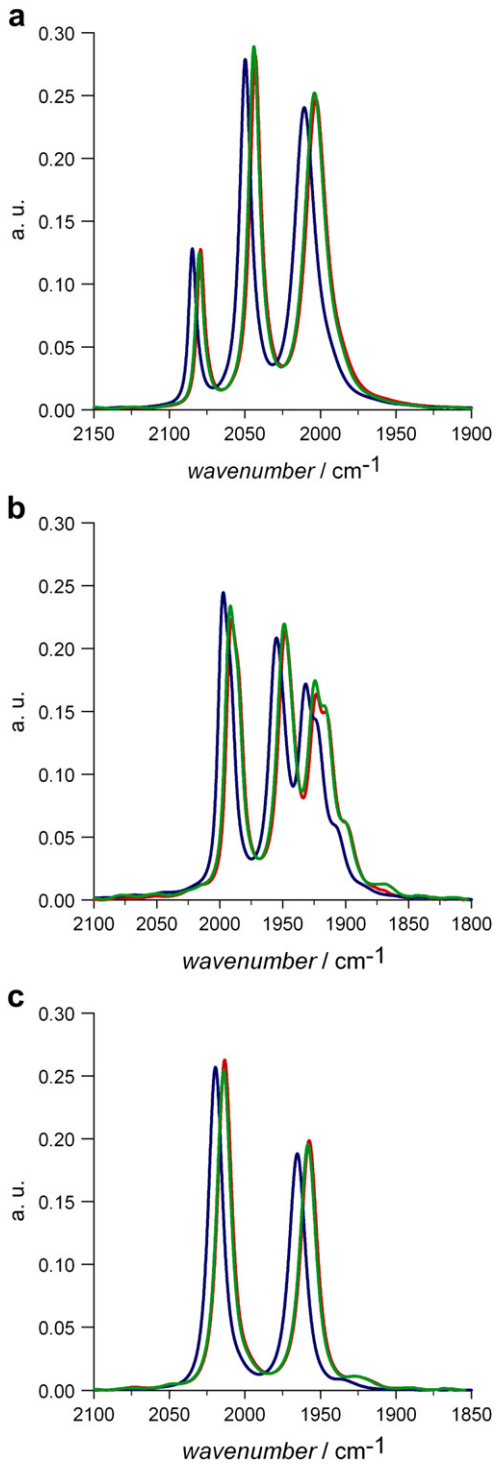

Fig. 2. The IR spectra (carbonyl region) of complexes (a) **1a** (green), **2a** (red) and **3a** (blue); (b) **1b** (green), **2b** (red) and **3b** (blue) and (c) **1c** (green), **2c** (red) and **3c** (blue) in CH_3CN. (For interpretation of the references to color in this figure legend, the reader is referred to the web version of this article.)

reaction between Fe_3CO_{12} and the respective arenedithiol, but also in more decomposition and lower yields. The ^1H NMR spectrum of **7a** shows the aromatic protons as two symmetric multiplets (AA′MM′ spin system) at $\delta = 7.71$ and 7.60 ppm. All aromatic carbons of the quinoxaline moiety feature in the $^{13}C\{^1H\}$ NMR spectrum as four signals together with the signal from the carbonyl carbons.

The shape of the carbonyl bands in the IR spectrum of **7a** is very similar to those in the spectra of (**1**–**3**)**a** (Fig. 3a). Compared to the CO stretching frequencies of **1a**, the corresponding bands in the IR spectrum of **7a** are, however, shifted by $\Delta\upsilon_{CO} = \sim 9\ cm^{-1}$ towards higher energy.

In the same manner as in the syntheses of (**1**–**3**)**b** and (**1**–**3**)**c**, **7a** was treated with trimethylphosphine to yield complexes **7b**, (Scheme 4). Noteworthy is that the reaction went to completion within 10 min, which is a remarkably short time considering that the reaction between the related $[Fe_2(\mu\text{-pdt})(CO)_6]$ (pdt = 1,3-propanedithiolate) and trimethylphosphine requires refluxing overnight to afford $Fe_2(\mu\text{-pdt})(CO)_4(PMe_3)_2$ [33]. When comparing the rate for the reaction between complexes (**1**–**3**,**7**)**a** and PMe_3, there is a clear correlation with the electron-withdrawing strength of the bridging dithiolate ligand. This is comprehensible as a more electron-withdrawing bridging ligand will decrease the electron density at the diiron core and thus make the iron centers more electrophilic. As a consequence, ligand substitutions with strong σ-donating ligands such as PMe_3 will be facilitated.

The ^1H NMR spectrum of **7b** exhibits a doublet at $\delta = 1.50$ ppm ($^2J_{H-P} = 8.8$ Hz) for the PMe_3 protons. The $^{31}P\{^1H\}$ NMR spectrum shows only one signal ($\delta = 22.8$ ppm) for the two equivalent PMe_3 ligands. The $^{13}C\{^1H\}$ NMR spectrum shows a doublet ($\delta = 20.9$ ppm, $J_{C-P} = 28.4$ Hz) for the methyl carbons and a doublet for the carbonyl carbons ($\delta = 215.3$ ppm, $J_{C-P} = 13.1$ Hz), all in agreement with the assignments in the spectra of complexes (**1**–**3**)**b**.

The $^{31}P\{^1H\}$ NMR spectrum of **7c** features only one signal at $\delta = 12.7$ ppm, indicating equivalent PMe_3 ligands as for the other mononuclear complexes (**1**–**3**)**c**. The ^1H NMR spectrum of **7c** shows a signal with a virtual triplet splitting pattern at $\delta = 1.51$ ppm ($|^2J_{H-P} + {}^4J_{H-P}| = 7.8$ Hz) which is assigned to the methyl protons and similar to those found in the ^1H NMR spectra of (**1**–**3**)**c**. A virtual splitting pattern is also visible for the PMe_3 methyl carbon resonance in the $^{13}C\{^1H\}$ NMR spectrum at $\delta = 15.1$ ppm ($|J_{C-P} + {}^3J_{C-P}| = 32.2$ Hz). The $^{13}C\{^1H\}$ NMR carbonyl carbon resonance appears as a triplet at

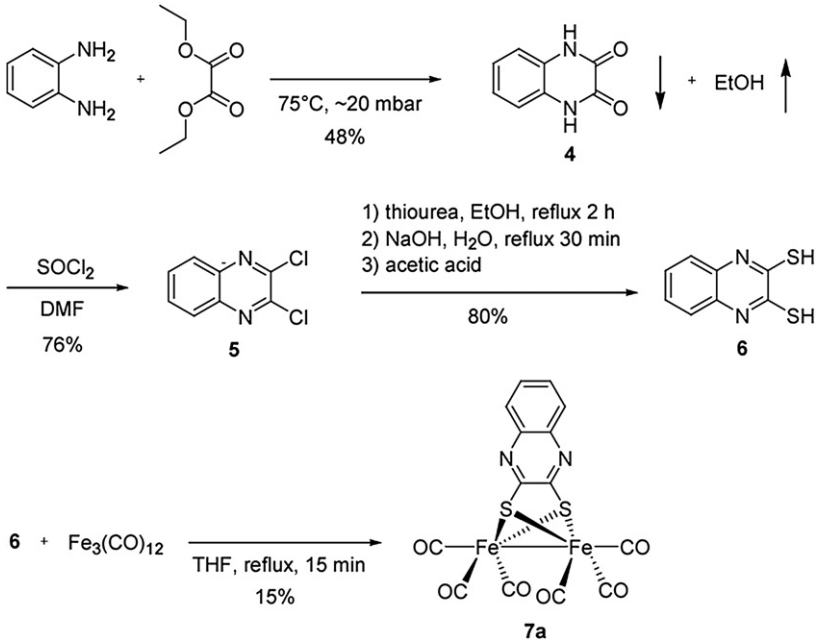

Scheme 3.

$\delta = 210.3$ ppm ($^2J_{C-P} = 22.3$ Hz), indicating that the PMe_3 ligands are in a *trans* and the CO ligands in *cis* position.

The IR spectra of complexes **7b** and **c** exhibit a similar pattern as **1b** and **c**, respectively. (Fig. 2b and c). Once more, the 2,3-quinoxalinedihiolate ligand in **7b** and **c** reveals its strong electron-withdrawing character compared to the 1,2-benzenedithiolate ligand by CO bands that are shifted to higher energy by $\Delta\upsilon_{CO} = \sim 11\ cm^{-1}$ compared to those in **1b** and **c**, respectively.

2.2. Crystal structures

The solid state structures of selected complexes were determined by single-crystal X-ray diffraction analysis. Crystallographic and metric data are summarized in Tables 1–4. The molecular structures of **1b**, **3a**, **3b**, **7b** and **7c** are presented in Figs. 4 and 5. The molecular structure of **1c** is found in the Supplementary material. As expected, the plane described by the arenedithiolate ligand resides in a symmetrical position orthogonal to the Fe–Fe bond vector in all structures. A comparison between the structures that belong to the same group of compounds (group **a**: $Fe_2(\mu\text{-}S_2Ar)(CO)_6$, **b**: $Fe_2(\mu\text{-}S_2Ar)(CO)_4(PMe_3)_2$ and **c**: $Fe(S_2Ar)(CO)_2(PMe_3)_2$ complexes) reveals that the Fe–Fe bond distances are rather constant and thus invariant to electronic modulations on the dithiolate ligands. In contrast, a lowered electron density at the diiron centers should decrease the extent of backbonding into the π^*-orbitals of the CO ligands and lead to shortened and stronger CO bonds. Similarly, the $Fe-C_{CO}$ bond order should decrease and the bond

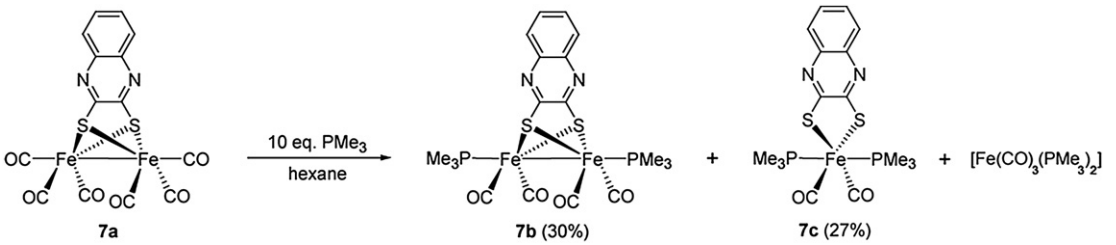

Scheme 4.

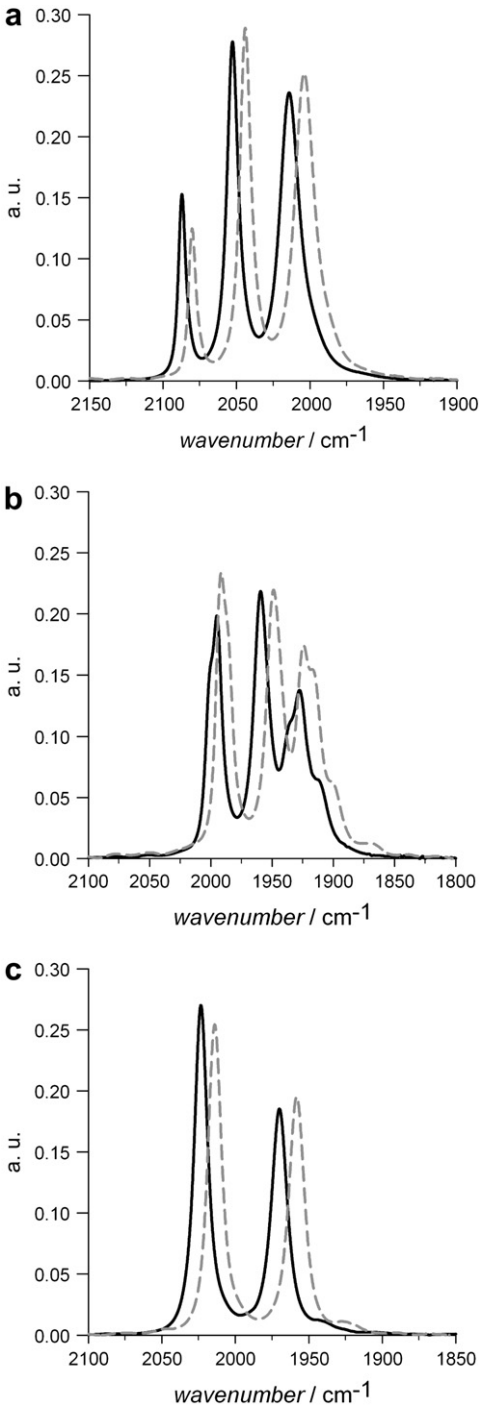

Fig. 3. The IR spectra (carbonyl region) of complexes (a) **1a** (grey, dashed) and **7a** (solid, black), (b) **1b** (dashed, grey) and **7b** (solid, black), (c) **1c** (dashed, grey) and **7c** (solid, black) in CH_3CN.

lengthens. We have recently demonstrated this effect on $[Fe_2(\mu\text{-}SC_2(BH)_{10}S)(CO)_6]$ [34], in which the unusually strong electron-withdrawing bridging *o*-carborene ligand gives rise to short ($d_{average} = 1.124(11)$ Å) carbon monoxide and long Fe−C_{CO} ($d_{average} = 1.799(17)$ Å) bond distances. Despite of the uncertainty errors that are associated with the crystallographic data of the compounds in groups **a** and **b**, there is a general trend towards longer Fe−C_{CO} and shorter C−O bond distances when more electron-withdrawing μ-arenedithiolates are employed as ligands.

In the solid state, two isomers of complex **3b** (Fig. 5c) cocrystallize in a monoclinic $P2_1$ space group. The two isomers differ mainly in the position of the two PMe_3 ligands. In **3b**$_{(ap,ap)}$, both phosphines reside in the apical position, whereas in the other isomer, **3b**$_{(ap,ba)}$, one of the PMe_3 ligands is in basal position. The two isomers are treated separately in Table 3. The structure of complex **7b** shows a somewhat distorted μ-quinoxaline-2,3-dithiolate moiety which may be explained by the steric demand of the bulky apical PMe_3 ligand. In contrast, however, this feature is not seen in **3b**$_{(ap,ba)}$ and the μ-benzenedithiolate ligand is not affected by the apical PMe_3 ligand.

*2.3. Electrochemical behavior of complexes (**1**–**3**)**a**, (**1**–**3**)**b**, (**1**–**3**)**c** and **7a**–**c***

The different arene moieties of the complexes are expected to influence the electron densities at the diiron centers and thus their reduction potentials. This effect can clearly be seen in the cyclic voltammograms (CH_3CN, $\nu = 0.1$ V/s) of complexes **1a**, **2a**, **3a** and **7a** (Fig. 6) which show reversible two-electron reductions for all complexes. As already indicated during the IR spectroscopic investigations in the previous section, the electron density at the diiron sites of complexes **3a** and **7a** is decreased compared to that of **1a**. As a consequence, the reductions of complexes **3a** and **7a** are thermodynamically more facile than that of complex **1a** by 110 and 130 mV, respectively (Table 5). The overall stoichiometry of the reduction process was determined by controlled-potential coulometry. From the inspection of Fig. 6, it is evident that all reductions are electrochemically and chemically reversible, except for that of complex **7a**. The voltammogram of **7a** features a shoulder after the expected re-oxidation wave in the reverse scan. Furthermore, the height of the re-oxidation wave is also less than that expected for a chemically reversible process. This behavior could be an indication that intermediate $\mathbf{7a}^{2-}$ is less stable than the analogous two-electron

reduction products of (**1**–**3**)**a**. Felton et al. have shown that the reduction of **1a** is a case of potential inversion, which means that it is thermodynamically easier to reduce $\mathbf{1a}^-$ than **1a**, leading to an overall two-electron reduction [14]. It is likely that the reductions of **2a**, **3a**, and **7a** follow a similar potential inversion mechanism.

Compared to the hexacarbonyl analogues, the electron-donating PMe_3 ligands shift the reductions of (**1**–**3**)**b** and **7b** by about 800 mV towards more negative potentials (Fig. 7 and Table 6). This shift is slightly higher than the difference in reduction potential between $Fe_2(\mu\text{-pdt})(CO)_4(PMe_3)_2$ and $Fe_2(\mu\text{-pdt})(CO)_6$ ($\Delta E_p^c = 0.61$ V) [35]. The strongly electron-withdrawing character of the arenedithiolates in **3b** and **7b** gives again rise to anodically shifted potentials compared to those required for the reduction of **1b** and **2b**. Compared to the complexes with the hexacarbonyl ligand set, this effect is even more pronounced in the generally electron richer $[Fe_2(\mu\text{-}S_2Ar)(CO)_4(PMe_3)_2]$. The electrochemical reversibility seen for complexes (**1**–**3**)**a** and **7a** is lost when the PMe_3 ligands are introduced in complexes (**1**–**3**)**b** and **7b**. Comparing the peak heights to those in the reduction of (**1**–**3**)**a** and **7a** and considering that the diffusion constant of these complexes is expected to be lower than the hexacarbonyl analogues suggests that the reduction of the bis-PMe_3 complexes is also an overall two-electron process. The mononuclear complexes **1c**, **2c**, **3c** and **7c** show a rather complicated electrochemical behavior that is the subject of ongoing investigations. Cyclic voltammograms and voltammetric data for complexes (**1**–**3**,**7**)**c** are found in the Supplementary material.

Table 1
Crystallographic data for complexes **1b**, **1c**, **3a**, **3b**, **7b** and **7c**

Code	**1b**	**1c**	**3a**	**3b**	**7b**	**7c**
Empirical formula	$C_{16}H_{22}Fe_2O_4P_2S_2$	$C_{14}H_{22}FeO_2P_2S_2$	$C_{12}H_2Cl_2Fe_2O_6S_2$	$C_{16}H_{20}Cl_2Fe_2O_4P_2S_2$	$C_{18}H_{22}Fe_2N_2O_4P_2S_2$	$C_{16}H_{22}FeN_2O_2P_2S_2$
Formula wt	516.10	404.23	488.86	585.00	568.14	456.27
Temperature (K)	293(2)	293(2)	293(2)	293(2)	293(2)	293(2)
Wavelength (Å)	Mo Kα (0.71073)	Mo Kα (0.71073)	Mo Kα (0.71073)	Mo Kα (0.71073)	Mo Kα (0.71073)	Mo Kα (0.71073)
Crystallographic system	Monoclinic	Orthorhombic	Monoclinic	Monoclinic	Orthorhombic	Monoclinic
Space group	$P2_1/n$	$P2_12_12_1$	$P2_1/c$	$P2_1$	$Pbca$	$C2/c$
a (Å)	10.1959(3)	8.7350(17)	8.6523(11)	11.1419(11)	28.846(12)	13.8024(4)
b (Å)	12.6987(4)	12.158(4)	12.301(2)	13.5340(18)	13.036(4)	13.1949(2)
c (Å)	17.4025(5)	17.988(4)	16.5832(18)	16.4695(15)	12.752(3)	12.8772(2)
α (°)	90	90	90	90	90	90
β (°)	93.139(3)	90	101.727(14)	92.951(11)	90	111.353(3)
γ (°)	90	90	90	90	90	90
V (Å^3)	2249.80(12)	1910.3(9)	1728.1(4)	2480.2(5)	4796(3)	2184.22(8)
Z, Z'	4, 1	4, 1	4, 1	4, 2	8,1	4,1
ρcalc (Mg/m^3)	1.524	1.405	1.879	1.567	1.574	1.387
μ (mm^{-1})	1.634	1.175	2.253	1.701	1.544	1.039
$F(000)$	1056	840	960	1184	2320	944
Size (mm)	0.10·0.20·0.25	0.20·0.25·0.30	0.10·0.15·0.40	0.05·0.10·0.30	0.08·0.20·0.35	0.05·0.15·0.25
T_{max}, T_{min}	0.85, 0.65	0.80, 0.70	0.79, 0.35	0.92, 0.56	0.88, 0.51	0.95, 0.65
$\theta_{min} - \theta_{max}$ (°)	3.78, 32.22	2.26, 27.91	2.40, 28.10	2.16, 26.37	2.11, 26.37	3.71, 33.08
N_{meas}	21 066	17 223	13 566	20 762	33 574	19 873
N_{unique}, R(int)	7289, 0.0625	4519, 0.0789	3772, 0.0907	10115, 0.1307	4891, 0.1230	3538, 0.0182
N_{obs}	2935	3966	2495	7717	3968	2647
Sign. criterion	$I > 2\sigma(I)$	$I > 2\sigma(I)$	$I > 2\sigma(I)$	$I > 2\sigma(I)$	$I > 2\sigma(I)$	$I > 2\sigma(I)$
No. of data/restr/par	7289/0/242	4519/0/197	3772/0/218	10115/195[c]/483	4891/0/4891	3538/0/118
Flack-parameter	–	−0.03(2)	–	0.59(3)	–	–
GOF	0.792	1.073	1.037	1.017	1.199	1.074
$R1$,[a] $wR2$[b] ($I > 2\sigma(I)$)	0.0382, 0.1324	0.0367, 0.0451	0.0489, 0.0823	0.0867, 0.2173	0.0697, 0.0876	0.0289, 0.0419
$R1$,[a] $wR2$[b] (all data)	0.0674, 0.0862	0.0877, 0.0981	0.1210, 0.1613	0.1060, 0.2372	0.1659, 0.1829	0.0815, 0.0887
Resid. Min, max (e Å^{-3})	−0.345, 0.346	−0.470, 0.659	−0.836, 0.682	−1.607, 1.086	−1.733, 0.860	-0.290, 0.308
Diffractometer	OD Exalibur	STOE IPDS	STOE IPDS	STOE IPDS	STOE IPDS	OD Exalibur
CCDC-number	676743	676742	676744	676745	676746	676747

[a] $R1 = \sum||F_o| - |F_c||/\sum|F_o|$.
[b] $wR2 = \{\sum[w(F_o^2 - F_c^2)^2]/\sum[w(F_o^2)^2]\}^{1/2}$.
[c] See Supplementary material.

Table 2
Selected bond lengths (Å) and bond angles (°) for **1a**, **2a** and **3a**

	1a[a]	**2a**[a]	**3a**
Fe(1)–Fe(2)	2.480(2)	2.4754(14)	2.480(9)
Fe(1)–S(1)	2.271(2)	2.269(2)	2.266(2)
Fe(1)–S(2)	2.272(2)	2.269(2)	2.267(3)
Fe(2)–S(1)	2.262(2)	2.271(2)	2.267(9)
Fe(2)–S(2)	2.267(2)	2.262(2)	2.256(10)
S(1)–C(7)	1.775(6)[d]	1.782[e]	1.784(16)
S(2)–C(12)	1.778(6)[d]	1.782[e]	1.776(8)
Fe–C_{CO}	1.792(8)[b]	1.774(8)[b]	1.797(13)[b]
C–O	1.135(8)[c]	1.139(8)[c]	1.128(10)[c]
S(1)–Fe(1)–S(2)	80.66(6)	80.44(7)	81.11(5)
S(1)–Fe(2)–S(2)	80.94(7)	80.47(7)	81.33(5)
Fe(1)–S(1)–Fe(2)	66.32(6)	66.09(6)	66.41(4)
Fe(1)–S(2)–Fe(2)	66.23(6)	66.30(6)	66.03(4)

[a] Data retrieved from the literature [19,21].
[b] Average over all six Fe–C_{CO} bonds.
[c] Average over all six C–O bonds.
[d] For comparative purposes, the labeling of specific atoms has been changed to be in agreement with the one in the structure of **3a**.
[e] Reported as an average value.

2.4. Electrochemical proton reduction

3,6-Dichloro-1,2-benzenedithiolate ligated complexes **3a**,**b** exhibit the mildest reduction potentials within their group and were therefore examined for their performance as electrochemical proton reduction catalysts. The cyclic voltammograms of **3a** with increasing amounts of trifluoromethanesulfonic acid demonstrate catalytic turnover similar to the data reported for **1a** (see Supplementary material) [13]. Considering the resemblance in these voltammograms, it is reasonable to assume that the catalysis follows the same mechanism. Since the reduction of **3a** is anodically shifted compared to that of **1a**, it is not surprising that turnover which follows an EECC mechanism that is catalyzed by **3a** proceeds at milder potentials than that required for the reaction that is catalyzed by **1a**. The cyclic voltammograms of complex **3b** with increasing concentrations of trifluoromethanesulfonic acid (HOTf) are shown in Fig. 8. Upon addition of HOTf, the Fe–Fe bond is protonated and $[(\mu\text{-H})3b]^+$ is formed. $[(\mu\text{-H})3b]^+$ has also been characterized by IR spectroscopy (see Supplementary material). Using similar conditions, a reduction wave emerges in the cyclic voltammograms at −1.07 V and the height of which first increases with increasing acid concentrations until it levels out. Since the current does not rise significantly beyond the current that is seen for the reduction of the complex in the absence of acid, catalytic proton reduction cannot be established from these cyclic voltammetry experiments.

Table 3
Selected bond lengths (Å) and bond angles (°) for **1b**, **3a**(ap,ap), **3a**(ap,ba) and **7b**

	1b	**3b**$_{(ap,ap)}$	**3b**$_{(ap,ba)}$	**7b**
Fe(1)–Fe(2)	2.472(3)	2.479(11)	2.535(11)	2.503(1)
Fe(1)–S(1)	2.291(1)	2.276(4)	2.283(3)	2.291(1)
Fe(1)–S(2)	2.299(2)	2.286(10)	2.278(3)	2.302(1)
Fe(2)–S(1)	2.291(1)	2.283(5)	2.271(10)	2.280(1)
Fe(2)–S(2)	2.295(1)	2.284(3)	2.288(8)	2.292(1)
S(1)–C(11)	1.794(3)	1.774(16)	1.766(11)	1.772(4)
S(2)–C(16)	1.789(4)	1.781(11)	1.776(7)	1.779(4)[a]
Fe–$C_{CO,\ ap}$	N/A	N/A	1.755(13)	1.769(5)
Fe–$C_{CO,\ ba}$	1.748(4)	1.763(13)[b]	1.752(14)[c]	1.761(5)[c]
C–O	1.158(5)	1.146(16)[d]	1.151(18)[e]	1.145(7)[e]
Fe(1)–P(1)	2.226(1)	2.226(3)	2.219(5)	2.205(1)
Fe(2)–P(2)	2.229(3)	2.220(11)	2.231(5)	2.224(1)
S(1)–Fe(1)–S(2)	80.41(3)	80.79(8)	80.79(9)	88.66(4)
S(1)–Fe(2)–S(2)	80.50(3)	80.71(8)	80.83(9)	82.11(4)
Fe(1)–S(1)–Fe(2)	65.29(2)	65.87(7)	67.64(8)	66.41(4)
Fe(1)–S(2)–Fe(2)	65.10(2)	65.70(7)	67.44(8)	66.03(4)

[a] S(2)–C(18).
[b] Average over all four Fe–C_{CO} bonds.
[c] Average over three Fe–$C_{CO,ba}$ bonds.
[d] Average over all four C–O bonds.
[e] Average over three basal CO ligand bonds.

Table 4
Selected bond lengths (Å) and bond angles (°) for **1c** and **7c**

	1c[a]	**7c**
Fe–S	2.302(1)[a]	2.303(1)
Fe–P	2.264(1)[a]	2.282(2)
S–C	1.756(3)[a]	1.742(1)
Fe–C_{CO}	1.770(3)[a]	1.760(2)
C–O	1.141(5)	1.146(2)
S(1)–Fe(1)–S(2)	89.65(3)	89.99(1)[b]
P(1)–Fe(1)–P(2)	174.61(4)	174.33(2)[c]

[a] Average value.
[b] S(1)–F(1)–S(1).
[c] P(1)–Fe(1)–P(1).

3. Conclusions

In summary, we have prepared four $[Fe_2(\mu\text{-}S_2Ar)(CO)_6]$ complexes that differ in the electron-donor ability of the bridging dithiolate ligand. IR spectroscopic, crystallographic and electrochemical investigations show that electron-withdrawing substituents on the ligand lead to a decreased electron density at the iron centers. Dinuclear complexes $[Fe_2(\mu\text{-}S_2Ar)(CO)_4(PMe_3)_2]$ (**1**–**3**,**7**)**b** and mononuclear complexes $[Fe(S_2Ar)(CO)_2(PMe_3)_2]$ (**1**–**3**,**7**)**c** were synthesized from $[Fe_2(\mu\text{-}S_2Ar)(CO)_6]$ by exposing the latter compounds to trimethylphosphine. Also in the

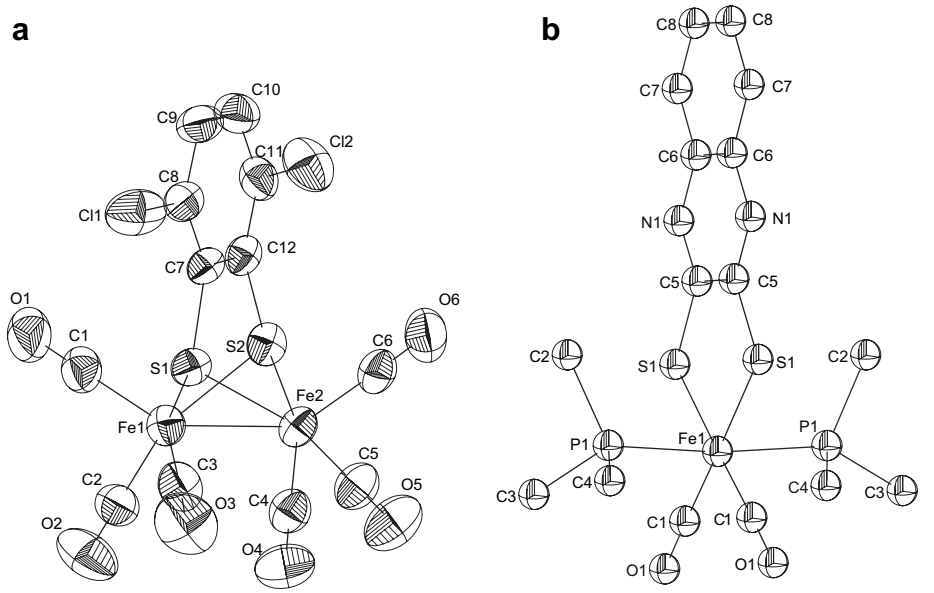

Fig. 4. Thermal ellipsoid representations (50% probability) of the molecular structures of (a) [Fe2(μ-3,6-dichloro-1,2-benzenedithiolate)(CO)6] (**3a**) and (b) [Fe(quinoxaline-2,3-dithiolate)$(CO)_2(PMe_3)_2$] (**7c**).

ligand-substituted compounds, the electronic properties of the diiron site can be tuned by choosing the appropriate aromatic ligand. The electron-withdrawing character of the ligand decreases in the order quinoxaline-2, 3-dithiolate > 3,6-dichloro-1,2-benzenedithiolate > 1, 2-benzenedithiolate ≥ toluene-3,4-dithiolate. Electrocatalytic proton reduction by complex **3a** was evidenced by cyclic voltammograms that are similar to those previously reported for **1a**. However, as a result of the milder reduction potential of **3a** itself, proton reduction that is promoted by **3a** proceeds at a potential that is milder than that for the **1a**-catalyzed process. The gain in potential presumably comes at the expense of the basicity of the reduced state in the catalytic cycle which we anticipate to be lower for $\mathbf{3a^{2-}}$ than for $\mathbf{1a^{2-}}$.

4. Experimental section

4.1. Materials

Solvents were of reagent grade and used without further purification unless otherwise noted. $Fe_3(CO)_{12}$ (Aldrich, containing 1–10% methyl alcohol), benzene-1,2-dithiol (Fluka, ≥95%), 3,6-dichloro-1,2-benzenedithiol (Sigma–Aldrich, 95%), toluene-3,4-dithiol (Fluka, ≥97%), trimethylphosphine (Fluka, ≥95%), and trifluoromethanesulfonic acid (Sigma–Aldrich, ≥99%) were purchased and used as received. Flash chromatography was performed on Merck silica gel SI-60Å (35–70).

4.2. NMR spectroscopy

^{1}H NMR spectra were recorded on a JEOL Eclipse + 400 MHz spectrometer (operating at 399.8 MHz) together with the JEOL Delta NMR Processing Software version 4.3 in acetonitrile or chloroform. Residual protic solvent peaks $CHCl_3$ ($\delta_H = 7.26$ ppm) were used as internal reference. ^{13}C NMR spectra were recorded on the same instrument operating at a frequency of 100.5 MHz using the central signals of $CDCl_3$ ($\delta = 77.16$ ppm) as reference signal. ^{31}P NMR spectra were also measured on a JEOL Eclipse + 400 MHz instrument at 161.8 MHz, with chemical shifts referenced to 85% H_3PO_4 as an external standard.

4.3. IR spectroscopy

IR absorption spectra were recorded between 1000 and 5000 cm^{-1} at a resolution of 1 cm^{-1} on a Bruker FT-IR spectrometer (IFS 66 v/S) with the sample as solution in a liquid–sample–cell (Bruker A140) between CaF_2 windows and a path length of 125 μm. The solutions were prepared in CH_3CN (Sigma–Aldrich, spectroscopic grade).

4.4. Electrochemistry

All electrochemical measurements were conducted in acetonitrile. Cyclic voltammetry and controlled-potential coulometry were carried out using an Autolab

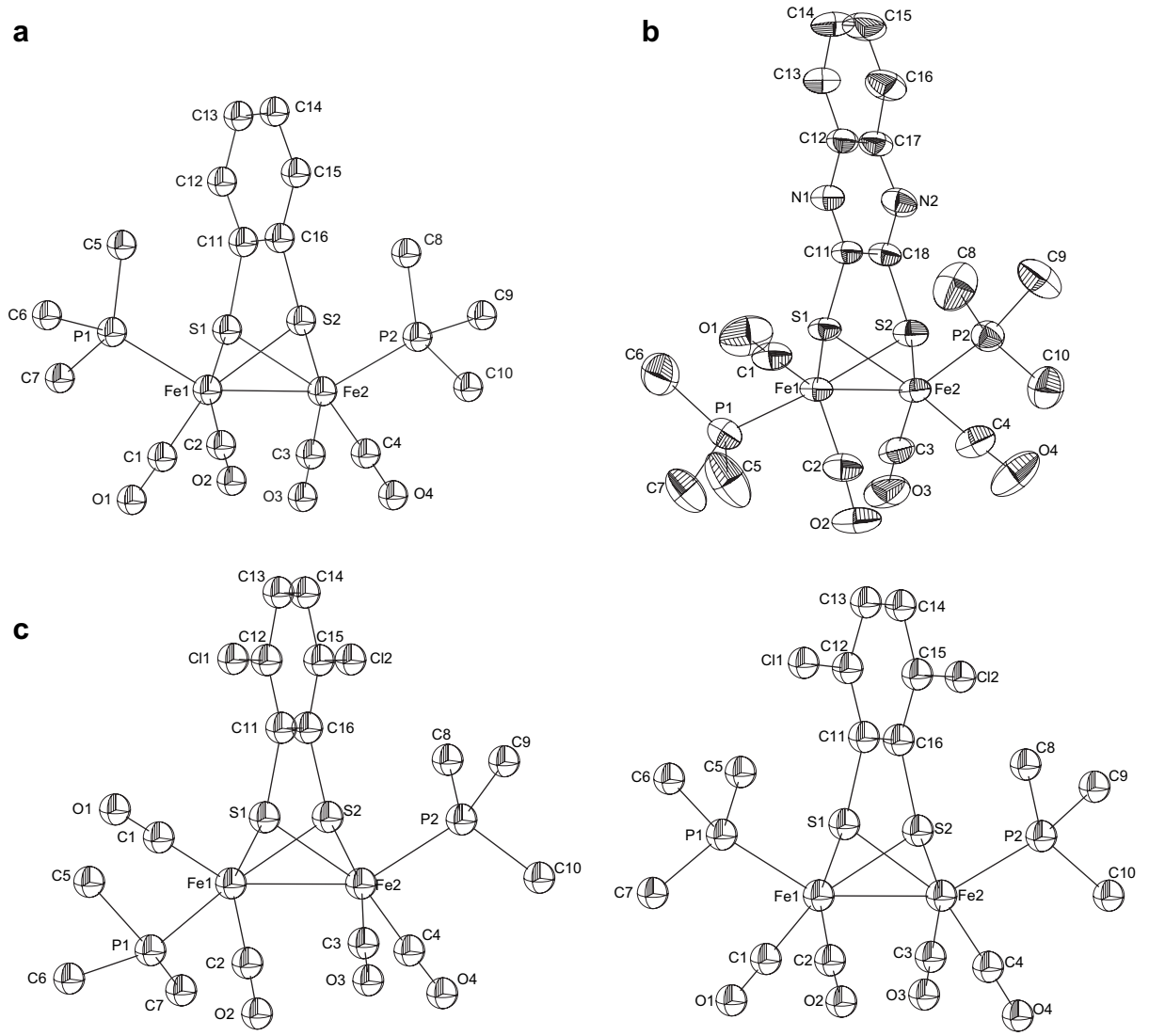

Fig. 5. Thermal ellipsoid representations (50% probability) of the molecular structures of (a) [Fe2(μ-1,2-benzenedithiolate)$(CO)_4(PMe_3)_2$] (**1b**), (b) [Fe_2(μ-quinoxaline-2,3-dithiolate)$(CO)_4(PMe_3)_2$] and (c) the two isomers of [Fe_2(μ-3,6-dichloro-1,2-benzenedithiolate)$(CO)_4(PMe_3)_2$]; $\mathbf{3b}_{ap,ba}$ (left) and $\mathbf{3b}_{ap,ap}$ (right).

potentiostat with a GPES electrochemical interface (Eco Chemie). The working electrode was a glassy carbon disc (diameter 3 mm, freshly polished) for voltammetry. For electrolysis experiments a platinum mesh was used. A glassy carbon rod in a compartment separated from the bulk solution by a fritted disk was used as counter electrode. The reference electrode was a non-aqueous Ag^+/Ag electrode (CH Instruments, 0.010 M $AgNO_3$ in acetonitrile) with a potential of −0.08 V vs. the ferrocenium/ferrocene (Fc^+/Fc) couple in acetonitrile as an external standard. All solutions were prepared from dry acetonitrile (Sigma–Aldrich, spectroscopic grade, dried with MS 3 Å) with 0.1 M tetrabutylammonium hexafluorophosphate (Fluka, electrochemical grade) as supporting electrolyte that was dried in vacuum at 383 K.

4.5. Single-crystal X-ray diffraction

Single-crystal X-ray diffraction patterns were recorded with either a Stoe IPDS diffractometer on a rotating anode Mo-radiation source ($\lambda = 0.71073$ Å) or an Oxford Diffraction Excalibur-II diffractometer on a sealed tube Mo-radiation source ($\lambda = 0.71073$ Å) with a Sapphire-II CCD detector. The type of diffractometer is given in Table 1. Indexing, cell refinements

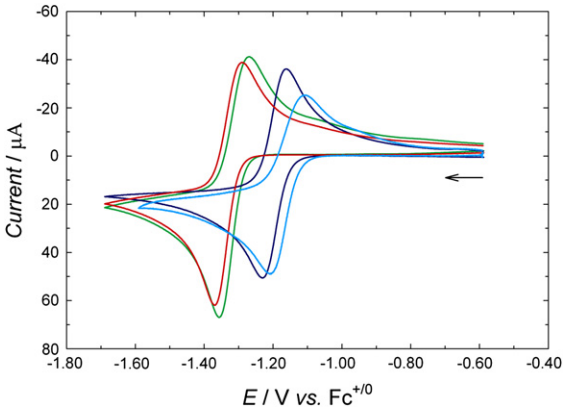

Fig. 6. Cyclic voltammograms ($v = 100$ mV/s) of **1a** (1.28 mM, green trace), **2a** (1.19 mM, red trace), **3a** (1.11 mM, navy blue trace) and **7a** (1.08 mM, cyan trace) in acetonitrile (0.1 M $(Bu)_4NPF_6$). (For interpretation of the references to color in this figure legend, the reader is referred to the web version of this article.)

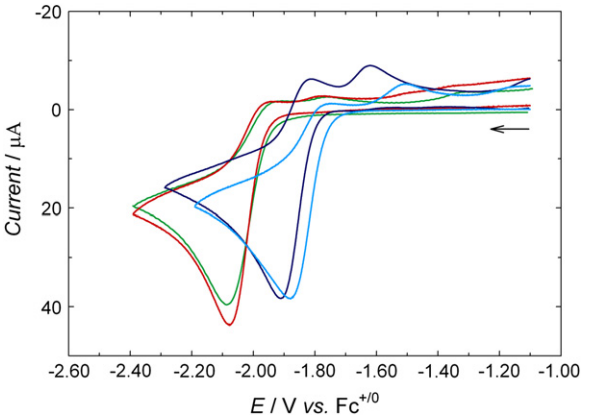

Fig. 7. Cyclic voltammograms ($v = 100$ mV/s) of **1b** (1.09 mM, green trace), **2b** (1.17 mM, red trace), **3b** (1.08 mM, navy blue trace) and **7b** (1.04 mM, cyan trace) in acetonitrile (0.1 M $(Bu)_4NPF6$). (For interpretation of the references to color in this figure legend, the reader is referred to the web version of this article.)

and integration of reflection intensities were performed with either the STOE IPDS software [36] or the Crystalis software [37]. Numerical absorption correction was performed with the program X-RED [38] using multiple measurements of symmetry equivalent reflections and verifying the crystal shape with program X-shape [39], for the STOE IPDS and with the Crystalis software [37] for the OD Excalibur diffractometer. The structures were solved by direct methods using SHELXS97 [40] giving electron density maps where most of the non-hydrogen atoms could be resolved. The rest of the non-hydrogen atoms were located from difference electron density maps and the structure model was refined with full matrix least square calculations on F^2 using the program SHELXL97-2 [41]. All non-hydrogen atoms were refined with anisotropic displacement parameters and the hydrogens, which were placed at geometrically calculated positions and let to ride on the atoms they were bonded to, were given isotropic displacement parameters calculated as ξU_{eq} for the non-hydrogen atoms with $\xi = 1.5$ for methyl hydrogens ($-CH_3$) and $\xi = 1.2$ for methylenic (CH_2), methinic (CH) and aromatic hydrogens.

Table 5
Cyclic voltammetric data (vs. $Fc^{+/0}$) for **1a**, **2a**, **3a** and **7a** at $v = 100$ mV/s in MeCN, containing 0.1 M $(Bu)_4NPF_6$

	1a	2a	3a	7a
E_p^c (V)	−1.36	−1.37	−1.23	−1.22
E_p^a (V)	−1.27	−1.29	−1.16	−1.13
$E_{1/2}^{red}$ (V)	−1.31[a]	−1.33	−1.20	−1.18
I_p^a/I_p^c	0.96	0.98	0.97	0.79

[a] Capon et al. have reported $E_{1/2} = -1.27$ V vs. $Fc^{+/0}$ [13]. Felton et al. have reported $E_{1/2} = -1.32$ V vs. $Fc^{+/0}$ [14].

4.6. Synthesis

4.6.1. [Fe_2(μ-1,2-benzenedithiolate)$(CO)_6$] (**1a**)

$Fe_3(CO)_{12}$ (1450 mg, 2.88 mmol) and 1,2-benzenedithiol (410 mg, 2.88 mmol) were dissolved in 20 mL of toluene. After reflux for 1.5 h under argon atmosphere, the solvent was removed by rotary evaporation. Purification by column chromatography yielded the pure product (685 mg, 57% yield). All spectroscopic data (^{1}H NMR, ^{13}C NMR, and IR) were in well agreement with the literature [19].

4.6.2. [Fe_2(μ-1,2-benzenedithiolate)$(CO)_4(PMe_3)_2$] (**1b**) and [Fe(1,2-benzenedithiolate)$(CO)_2(PMe_3)_2$] (**1c**)

Complex **1a** (530 mg, 1.26 mmol) and 15 mL of degassed hexane were added to an argon-filled Schlenk flask. After complete solvation, trimethylphosphine (670 μL, 12.6 mmol) was added dropwise. The dark red solution was stirred for 75 min and the solvents were removed *in vacuo*. Purification by flash column chromatography (using toluene as eluent) yielded two intense colored bands, where the first band eluted (red-brown) is **1b** and the second (red-magneta) is **1c**. Both products were recrystallized from hexane/toluene mixtures to obtain single crystals. Yield: **1b**: 325 mg (50%); **1c**: 128 mg (25%). **1b**: ^{1}H NMR

Table 6
Cyclic voltammetric data (vs. $Fc^{+/0}$) for **1b**, **2b**, **3b** and **7b** at $v = 100$ mV/s in MeCN, containing 0.1 M $(Bu)_4NPF_6$

	1b	2b	3b	7b
E_p^c (V)	−2.09	−2.08	−1.91	−1.88

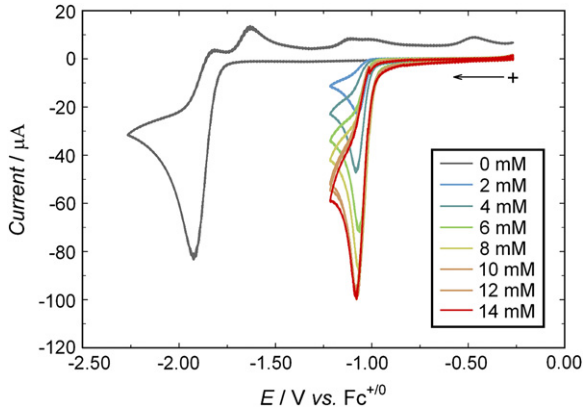

Fig. 8. Cyclic voltammograms ($\nu = 100$ mV/s) of complex **3b** (2 mM) on glassy carbon electrode in CH_3CN (0.1 M $(Bu)_4NPF_6$) solution with trifluoromethanesulfonic acid (0–14 mM). (For visualizing colors, see the web version of this article.)

(400 MHz, $CDCl_3$): $\delta = 7.02$ (m, 2H), 6.48 (m, 2H), 1.48 (d, $J_{H-P} = 8.8$ Hz, 18H) ppm; ^{13}C NMR (100 MHz, $CDCl_3$): $\delta = 216.4$ (d, $^2J_{C-P} = 10.8$ Hz), 151.8, 127.5, 125.2, 20.8 (d, $J_{C-P} = 26.1$ Hz) ppm; ^{31}P NMR (161.9 MHz, $CDCl_3$): $\delta = 20.9$ ppm. IR (CH_3CN, cm^{-1}): $\upsilon_{CO} = 1992$ (s), 1986 (sh), 1949 (s), 1924 (m), 1917 (m), 1900 (sh), 1968 (vw). Anal. Calcd for $C_{16}H_{22}Fe_2O_4P_2S_2$: C, 37.23; H, 4.30. Found: C, 37.34; H, 4.35%. **1c**: ^1H NMR (400 MHz, $CDCl_3$): $\delta = 7.19$ (m, 2H), 6,69 (m, 2H), 1.45 (t′, $|^2J_{H-P} + {}^4J_{H-P}| = 8.0$ Hz, 18H); ^{13}C NMR (100 MHz, $CDCl_3$): $\delta = 211.3$ (t, $^2J_{C-P} = 21.5$ Hz), 146.8, 128.4, 122.1, 14.4 (t′, $|^1J_{C-P} + {}^3J_{C-P}| = 30.8$ Hz) ppm; ^{31}P NMR (161.9 MHz, $CDCl_3$): $\delta = 11.3$ ppm. IR (CH_3CN, cm^{-1}): $\upsilon_{CO} = 2014$ (s), 1958 (s), 1924 (vbr). Anal. Calcd. for $C_{14}H_{22}FeO_2P_2S_2$: C, 41.60; H, 5.49. Found: C, 41.27; H, 5.64%.

4.6.3. *[Fe_2(μ-toluene-3,4-dithiolate)$(CO)_6$] (**2a**)*

$Fe_3(CO)_{12}$ (3.80 g, 7.54 mmol) and toluene-3, 4-dithiol (1180 mg, 7.54 mmol) were dissolved in 40 mL of toluene. The reaction mixture was refluxed for 1.5 h under argon atmosphere. The solvent was removed by rotary evaporation and purification by column chromatography yielded the pure product (1.67 g, 51% yield). All spectroscopic data (^1H NMR, ^{13}C NMR, and IR) were in agreement with the literature [20,21].

4.6.4. *[Fe_2(μ-toluene-3,4-dithiolate)$(CO)_4(PMe_3)_2$] (**2b**) and [Fe(toluene-3,4-dithiolate)$(CO)_2(PMe_3)_2$] (**2c**)*

Complex **2a** (608 mg, 1.40 mmol) and 10 mL of degassed hexane were added to an argon-filled Schlenk flask. After complete solvation, trimethylphosphine (750 μL, 14.0 mmol) was added dropwise. The dark red solution was stirred for 1.5 h and the solvents were removed *in vacuo*. Purification by flash column chromatography (toluene/pentane = 50/50) yielded two intense colored bands, where the first band eluted (red-brown) is **2b** and the second (red-magneta) is **2c**. Both products were recrystallized from hexane/toluene mixtures to obtain single crystals. Yield: **2b**: 193 mg (26%); **2c**: 125 mg (21%). **2b**: ^1H NMR (400 MHz, $CDCl_3$): $\delta = 6.90$ (s, 1H), 6.87 (d, $J = 7.6$ Hz, 1H), 6.26 (d, $J = 7.3$ Hz, 1H), 2.02 (s, 3H), 1.48 (d, $J_{H-P} = 9.2$ Hz, 18H) ppm; ^{13}C NMR (100 MHz, $CDCl_3$): $\delta = 216.5$ (d, $^2J_{C-P} = 10.8$ Hz), 151.8, 148.1, 135.1, 128.6, 127.1, 125.6, 20.8 (d, $^2J_{C-P} = 26.9$ Hz) ppm; ^{31}P NMR (161.9 MHz, $CDCl_3$): $\delta = 21.1$ ppm. IR (CH_3CN, cm^{-1}): $\upsilon_{CO} = 1991$ (s), 1986 (sh), 1948 (s), 1923 (m), 1916 (m), 1899 (sh). Anal. Calcd for $C_{17}H_{24}Fe_2O_4P_2S_2$: C, 38.51; H, 4.56. Found: C, 38.69; H, 4.65%. **2c**: ^1H NMR (400 MHz, $CDCl_3$): $\delta = 7.06$ (d, $J = 7.7$ Hz, 1H), 7.02 (s, 1H), 6.51 (d, $J = 7.7$ Hz, 1H), 2.14 (s, 3H), 1.45 (t′, $|^2J_{H-P} + {}^4J_{H-P}| = 8.0$ Hz, 18H); ^{13}C NMR (100 MHz, $CDCl_3$): $\delta = 211.3$ (t, $^2J_{C-P} = 21.1$ Hz), 211.3 (t, $^2J_{C-P} = 21.1$ Hz), 146.7, 143.0, 131.7, 129.1, 128.0, 123.4, 20.6, 14.5 (t′, $|^1J_{C-P} + {}^3J_{C-P}| = 30.8$ Hz) ppm; ^{31}P NMR (161.9 MHz, $CDCl_3$): $\delta = 11.2$ ppm. IR (CH_3CN, cm^{-1}): $\upsilon_{CO} = 2014$ (s), 1958 (s), 1925 (vbr). Anal. Calcd for $C_{15}H_{24}FeO_2P_2S_2$: C, 43.07; H, 5.78. Found: C, 42.94; H, 5.96%.

4.6.5. *[Fe_2(μ-3,6-dichloro-1,2-benzenedithiolate)$(CO)_6$] (**3a**)*

$Fe_3(CO)_{12}$ (1.45 g, 2.88 mmol) and 3,6-dichloro-1, 2-benzenedithiol (610 mg, 2.88 mmol) were dissolved in 45 mL of toluene. The green reaction mixture was refluxed under argon atmosphere for 45 min. After removal of solvent by rotary evaporation, column chromatography (using hexane as eluent) was performed to obtain the pure product. Recrystallization from a mixture of hexane and toluene yielded single crystals. Yield: 25%. ^1H NMR (400 MHz, $CDCl_3$): $\delta = 6.63$ (s, 2H) ppm; ^{13}C NMR (100 MHz, $CDCl_3$): $\delta = 206.9$, 148.9, 132.3, 129.7 ppm. IR (CH_3CN, cm^{-1}): $\upsilon_{CO} = 2085$ (m), 2050 (s), 2011 (s). Anal. Cald for $C_{12}H_2Cl_2Fe_2O_6S_2$: C, 29.48; H, 0.41. Found: C, 29.62; H, 0.52%.

4.6.6. *[Fe_2(μ-3,6-dichloro-1,2-benzenedithiolate)$(CO)_4(PMe_3)_2$] (**3b**) and [Fe(3,6-dichloro-1, 2-benzenedithiolate)$(CO)_2(PMe_3)_2$] (**3c**)*

Complex **3a** (260 mg, 0.53 mmol) and 8 mL of degassed hexane were added to an argon-filled Schlenk

flask. After complete solvation, trimethylphosphine (280 μL, 5.3 mmol) was added dropwise. The dark red solution was stirred for 45 min and the solvents were removed *in vacuo*. Purification by flash column chromatography (toluene/hexane = 40/60) yielded two intense colored bands, where the first band eluted (red-brown) is **3b** and the second (red-magneta) is **3c**. Both products were recrystallized from hexane/toluene mixtures to obtain single crystals. Yield: **3b**: 83 mg (27%); **3c**: 85 mg (34%). **3b**: ^{1}H NMR (400 MHz, $CDCl_3$): $\delta = 6.49$ (s, 2H), 1.53 (d, $J_{H-P} = 9.2$ Hz, 18H) ppm; ^{13}C NMR (100 MHz, $CDCl_3$): $\delta = 215.8$ (d, $^{2}J_{C-P} = 10.8$ Hz), 153.5, 132.0, 127.5, 21.0 (d, $^{2}J_{C-P} = 26.9$ Hz) ppm; ^{31}P NMR (161.9 MHz, $CDCl_3$): $\delta = 21.2$ ppm. IR (CH_3CN, cm^{-1}): $\upsilon_{CO} = 1997$ (s), 1991 (sh), 1955 (s), 1932 (m), 1924 (sh), 1908 (sh). Anal. Calcd for $C_{16}H_{20}Cl_2Fe_2O_4P_2S_2$: C, 32.85; H, 3.45. Found: C, 32.99; H, 3.44%. **3c**: ^{1}H NMR (400 MHz, $CDCl_3$): $\delta = 6.75$ (s, 2H), 1.47 (t′, $|^{2}J_{H-P} + {}^{4}J_{H-P}| = 8.0$ Hz, 18H) ppm; ^{13}C NMR (100 MHz, $CDCl_3$): $\delta = 210.7$ (t, $^{2}J_{C-P} = 22.3$ Hz), 148.4, 131.1, 124.0, 14.4 (t′, $|^{1}J_{C-P} + {}^{3}J_{C-P}| = 31.6$ Hz) ppm; ^{31}P NMR (161.9 MHz, $CDCl_3$): $\delta = 11.9$ ppm. IR (CH_3CN, cm^{-1}): $\upsilon_{CO} = 2020$ (s), 1965 (s), 1939 (sh). Anal. Calcd for $C_{14}H_{20}Cl_2FeO_2P_2S_2$ * 15% of toluene: C, 37.39; H, 4.41. Found: C, 37.55; H, 4.62%.

4.6.7. 1,4-Dihydro-quinoxaline-2,3-dione (*4*)

Complex **4** was prepared according to the literature procedure of Lin [30]. 1,2-Phenyldiamine 15.73 g (145 mmol) was added to 60 mL of diethyl oxalate. The reaction mixture was stirred at water aspirator pressure (20 mbar) and 70 °C overnight. The yellow-brown precipitate was filtrated, washed several times with Et_2O and dried *in vacuo* to yield an off-white solid. Yield: 11.6 g (48%). The ^{1}H NMR and ^{13}C NMR spectra of **4** were in agreement with the literature.

4.6.8. 2,3-Dichloroquinoxaline (*5*)

The procedure was adapted from Komin et al. [31]. Complex **4** 11.5 g (69.1 mmol) was added to a mixture of 40 mL of thionyl chloride and 1.5 mL of DMF. The suspension was refluxed for 20 min and another 75 mL of thionyl chloride and 3 mL of DMF were added. After reflux for an additional 1.5 h, a clear solution had been formed. The solvents were removed by vacuum distillation, first at atmosphere pressure, then at aspirator vacuum and finally high vacuum. The remaining solid was poured over ice, filtrated, washed with water and dried. Yield: 9.87 g (76%). ^{1}H NMR (400 MHz, $CDCl_3$): $\delta = 8.03$ (m, 2H), 7.81 (m, 2H) ppm;. ^{13}C NMR (100 MHz, $CDCl_3$): $\delta = 145.5$, 140.7, 131.4, 128.4 ppm.

4.6.9. Quinoxaline-2,3-dithiol (*6*)

Complex **6** was prepared according to the literature procedure of Morrison and Furst [32]. Complex **5** 4.00 g (20.1 mmol) was added to 100 mL of absolute alcohol. Thiourea 8.00 g (105 mmol) was added and the reaction mixture was refluxed for 2 h. The volume was reduced and the remaining slurry was treated with 100 mL of H_2O and a solution of 25 g of NaOH in 150 mL. The yielded orange slurry was refluxed for 30 min and was immediately filtrated. The orange filtrate was acidified with acetic acid and a brown-red product was formed which was filtrated off. The product was washed with H_2O several times and twice with Et_2O and then dried. Yield: 80%. The product was used without further purification or analysis.

4.6.10. [Fe_2(μ-quinoxaline-2,3-dithiolate)$(CO)_6$] (*7a*)

Quinoxaline-2,3-dithiol (**6**) 730 mg (3.75 mmol) and 50 mL of degassed THF were added to an 100 mL round-bottomed flask. To the brown-green slurry, 1888 mg (3.75 mmol) of triiron dodecacarbonyl was added. The round-bottomed flask was equipped with a condenser and the system was flushed with argon. The reaction mixture was refluxed under argon atmosphere for 15 min. After cooling to room temperature, the solvent was removed by rotary evaporation. Purification by column chromatography (using toluene as eluent) and then recrystallization from hexane/toluene solutions yielded the pure product in 15% (276 mg) yield. ^{1}H NMR (400 MHz, $CDCl_3$): $\delta = 7.71$ (m, 2H), 7.60 (m, 2H) ppm; ^{13}C NMR (100 MHz, $CDCl_3$): $\delta = 206.4$, 164.0, 137.4, 131.3, 128.4 ppm. IR (CH_3CN, cm^{-1}): $\upsilon_{CO} = 2087$ (m), 2053 (s), 2014 (s). Anal. Calcd for $C_{14}H_4Fe_2N_2O_6S_2$: C, 35.62; H, 0.85. Found: C, 35.81; H, 0.98%.

4.6.11. [Fe_2(μ-quinoxaline-2,3-dithiolate)$(CO)_4(PMe_3)_2$] (*7b*) and [Fe(quinoxaline-2,3-dithiolate)$(CO)_2(PMe_3)_2$] (*7c*)

Complex **7a** (400 mg, 0.85 mmol) and 12 mL of degassed hexane were added to an argon-filled Schlenk flask. After complete solvation, trimethylphosphine (450 μL, 8.5 mmol) was added dropwise. The dark red solution was stirred for 10 min and the solvents were removed *in vacuo*. Purification by flash column chromatography (using first toluene and then toluene/acetone (90/10) as eluent) yielded two intense colored

bands, where the first band eluted (red) is **7b** and the second (yellow) is **7c**. Both products were recrystallized from hexane/toluene mixtures to obtain single crystals. Yield: **7b**: 144 mg (30%); **7c**: 105 mg (27%). **7b**: ^{1}H NMR (400 MHz, $CDCl_3$): $\delta = 7.59$ (m, 2H), 7.45 (m, 2H), 1.50 (d, $^{2}J_{H-P} = 18$H) ppm; ^{13}C NMR (100 MHz, $CDCl_3$): $\delta = 215.3$ (d, $^{2}J_{C-P} = 13.1$ Hz), 169.8, 137.2, 129.7, 20.9 (d, $^{2}J_{C-P} = 28.4$ Hz) ppm; ^{31}P NMR (161.9 MHz, $CDCl_3$): $\delta = 22.8$ ppm. IR (CH_3CN, cm^{-1}): $\upsilon_{CO} = 2000$ (sh), 1995 (s), 1960 (s), 1935 (sh), 1928 (m), 1912 (sh). Anal. Calcd for $C_{18}H_{22}Fe_2N_2O_4P_2S_2$: C, 38.05; H, 3.90. Found: C, 37.88; H, 3.90%. **7c**: ^{1}H NMR (400 MHz, $CDCl_3$): $\delta = 7.65$ (m, 2H), 7.32 (m, 2H), 1.51 (t′, $|^{2}J_{H-P} + {}^{4}J_{H-P}| = 7.8$ Hz, 18H) ppm; ^{13}C NMR (100 MHz, $CDCl_3$): $\delta = 210.3$ (t, $^{2}J_{C-P} = 22.3$ Hz), 168.9, 137.9, 126.5, 126.4, 15.1 (t′, $|^{1}J_{C-P} + {}^{3}J_{C-P}| = 32.2$ Hz) ppm; ^{31}P NMR (161.9 MHz, $CDCl_3$): $\delta = 12.7$ ppm. IR (CH_3CN, cm^{-1}): $\upsilon_{CO} = 2024$ (s), 1970 (s), 1939 (vbr). Anal. Cald for $C_{16}H_{22}FeN_2O_2P_2S_2$: C, 42.12; H, 4.86. Found: C, 42.22; H, 4.98%.

Acknowledgement

Financial support for this work was provided by the Swedish Research Council, the Swedish Energy Agency, the Knut and Alice Wallenberg Foundation and EU/Energy project SOLAR-H2 (contract # 212508).

Appendix. Supplementary material

Molecular structure of **1c**; cyclic voltammetry and voltammetric data for complexes (**1**–**3**,**7**)**c**; cyclic voltammograms of **3a** (with increasing amounts of trifluoromethanesulfonic acid); IR spectrum of $[(\mu\text{-H})3b]^{+}$ are found in the Supplementary material. The X-ray crystallographic data have been deposited with the Cambridge Crystallographic Data Center for complexes **1b** (CCDC no. 676743), **1c** (CCDC no. 676742), **3a** (CCDC no. 676744), **3b** (CCDC no. 676745), **7b** (CCDC no. 676746), and **7c** (CCDC no. 676747).

Supplementary data associated with this article can also be found in the online version, at doi: 10.1016/j.crci.2008.04.001.

References

[1] M.W.W. Adams, Biochim. Biophys. Acta 1020 (1990) 115.
[2] J.W. Peters, W.N. Lanzilotta, B.J. Lemon, L.C. Seefeldt, Science 282 (1998) 1853.
[3] Y. Nicolet, C. Piras, P. Legrand, C.E. Hatchikian, J.C. Fontecilla-Camps, Structure 7 (1999) 13.
[4] C. Tard, X.M. Liu, S.K. Ibrahim, M. Bruschi, L. De Gioia, S.C. Davies, X. Yang, L.S. Wang, G. Sawers, C.J. Pickett, Nature 433 (2005) 610.
[5] L. Schwartz, G. Eilers, L. Eriksson, A. Gogoll, R. Lomoth, S. Ott, Chem. Commun. (2006) 520.
[6] I.P. Georgakaki, L.M. Thomson, E.J. Lyon, M.B. Hall, M.Y. Darensbourg, Coord. Chem. Rev. 238 (2003) 255.
[7] D.J. Evans, C.J. Pickett, Chem. Soc. Rev. 32 (2003) 268.
[8] L.C. Sun, B. Akermark, S. Ott, Coord. Chem. Rev. 249 (2005) 1653.
[9] J.F. Capon, F. Gloaguen, P. Schollhammer, J. Talarmin, Coord. Chem. Rev. 249 (2005) 1664.
[10] T.B. Rauchfuss, Inorg. Chem. 43 (2004) 14.
[11] L.C. Song, Acc. Chem. Res. 38 (2005) 21.
[12] G.A.N. Felton, R.S. Glass, D.L. Lichtenberger, D.H. Evans, Inorg. Chem. 45 (2006) 9181.
[13] J.F. Capon, F. Gloaguen, P. Schollhammer, J. Talarmin, J. Electroanal. Chem. 595 (2006) 47.
[14] G.A.N. Felton, A.K. Vannucci, J. Chen, L.T. Lockett, N. Okumura, B.J. Petro, U.I. Zakai, D.H. Evans, R.S. Glass, D.L. Lichtenberger, J. Am. Chem. Soc. 129 (2007) 12521.
[15] H.K. Joshi, J.J.A. Cooney, F.E. Inscore, N.E. Gruhn, D.L. Lichtenberger, J.H. Enemark, Proc. Natl. Acad. Sci. USA 100 (2003) 3719.
[16] H.K. Joshi, J.H. Enemark, J. Am. Chem. Soc. 126 (2004) 11784.
[17] J.J.A. Cooney, M.A. Cranswick, N.E. Gruhn, H.K. Joshi, J.H. Enemark, Inorg. Chem. 43 (2004) 8110.
[18] J.S. McKennis, E.P. Kyba, Organometallics 2 (1983) 1249.
[19] J.A. Cabeza, M.A. Martinez-Garcia, V. Riera, D. Ardura, S. Garcia-Granda, Organometallics 17 (1998) 1471.
[20] R.B. King, J. Am. Chem. Soc. 85 (1963) 1584.
[21] M.M. Hasan, M.B. Hursthouse, S.E. Kabir, K.M.A. Malik, Polyhedron 20 (2001) 97.
[22] X. Zhao, I.P. Georgakaki, M.L. Miller, R. Mejia-Rodriguez, C.Y. Chiang, M.Y. Darensbourg, Inorg. Chem. 41 (2002) 3917.
[23] D. Sellmann, E. Unger, Z. Naturforsch., B 34 (1979) 1096.
[24] D. Sellmann, U. Kleinekleffmann, L. Zapf, G. Huttner, L. Zsolnai, J. Organomet. Chem. 263 (1984) 321.
[25] T.B. Rauchfuss, S.M. Contakes, S.C.N. Hsu, M.A. Reynolds, S.R. Wilson, J. Am. Chem. Soc. 123 (2001) 6933.
[26] R.K. Harris, Can. J. Chem. 42 (1964) 2275.
[27] R.H. Crabtree, The Organometallic Chemistry of the Transition Metals, fourth ed., Wiley, New York, 2005.
[28] R.J. Abraham, H.J. Bernstein, Can. J. Chem. 39 (1961) 216.
[29] D.S. Chong, I.P. Georgakaki, R. Mejia-Rodriguez, J. Samabria-Chinchilla, M.P. Soriaga, M.Y. Darensbourg, Dalton Trans. (2003) 4158.
[30] S.-K. Lin, Molecules 1 (1996) 37.
[31] A.P. Komin, M. Carmack, J. Heterocycl. Chem. 13 (1976) 13.
[32] D.C. Morrison, A. Furst, J. Org. Chem. 21 (1956) 470.
[33] X. Zhao, I.P. Georgakaki, M.L. Miller, J.C. Yarbrough, M.Y. Darensbourg, J. Am. Chem. Soc. 123 (2001) 9710.
[34] L. Schwartz, L. Eriksson, R. Lomoth, F. Teixidor, C. Viñas, S. Ott, Dalton Trans. (2008) 2379 (advanced article).
[35] F. Gloaguen, J.D. Lawrence, M. Schmidt, S.R. Wilson, T.B. Rauchfuss, J. Am. Chem. Soc. 123 (2001) 12518.

[36] STOE IPDS Diffractometer Control Software, 1997, Version 2.87. Stoe & Cie GmbH, Darmstadt, Germany.
[37] CrysAlis Software System, CCD and RED, Version 1.170, Oxford Diffraction, 2003.
[38] X-Red, Absorption Correction Program, Version 1.09, 1997, Stoe & Cie GmbH, Darmstadt, Germany.
[39] X-Shape, Crystal Optimisation for Numerical Absorption Correction, 1997, Version 1.2, Stoe & Cie GmbH, Darmstadt, Germany.
[40] G.M. Sheldrick, Acta Crystallogr. A46 (1990) 467.
[41] G.M. Sheldrick, Computer Program for the Refinement of Crystal Structures, Göttingen, Germany, 1997.